International Journal of Refrigeration 110 (2020) 196–207

Contents lists available at ScienceDirect

International Journal of Refrigeration

journal homepage: www.elsevier.com/locate/ijrefrig

Study on dynamic thermal performance and optimization of hybrid systems with capillary mat cooling and displacement ventilation

Nan Li[a,b], Qiong Chen[a,b,*]

[a] National Centre for International Research of Low-carbon and Green Buildings, Ministry of Science & Technology, Chongqing University, Chongqing 400044, China

[b] Joint International Research Laboratory of Green Buildings and Built Environments, Ministry of Education, Chongqing University, Chongqing 400044, China

ARTICLE INFO

Article history:
Received 9 March 2019
Revised 24 September 2019
Accepted 16 October 2019
Available online 19 October 2019

Keywords:
Response time
Hybrid system
Capillary mat
Displacement ventilation
Orthogonal experiment
Heat transfer coefficient

ABSTRACT

In this paper, the thermal performance of capillary mat cooling systems is evaluated through actual measurements under different ventilation rates. The results showed that the indoor air temperature drop rates of the ceiling, wall and floor cooling are 1.42–2.44 °C/h, 0.69–1.11 °C/h, 0.29–0.58 °C/h, respectively, in the response phase, which can provide a reference for predictive control strategy of radiant system. Then the cooling capacity of the capillary mat is validated. The radiant heat transfer coefficient of the cooling capillary mat is about 5.80 W/m^2 k. When the supply water temperature dropped from 20 °C to 16 °C, the total heat flux can experience an increase of 10%–30%. The heat flux for cooling ceilings is the largest, followed by cooling walls, which is 7%–17% lower; and cooling floors, which is 75%–90% lower. Orthogonal experiments illustrated that the water supply temperature and air supply volume have a significant influence on the indoor thermal environment of the hybrid systems, followed by the air supply temperature. In general, the dynamic performance of the radiant cooling system in the response phase can provide an effective reference for different control strategy considering the significant thermal inertia.

Étude sur les performances thermiques dynamiques et l'optimisation de systèmes hybrides avec refroidissement par matelas capillaire et ventilation par déplacement

Mots clés: Temps de réponse; Système hybride; Tapis/matelas capillaire; Ventilation par déplacement; Expérience orthogonale; Coefficient de transfert de chaleur

1. Introduction

Global warming, as one of the environmental problems, has deteriorated the quality of life and health of people, prompting the concept of energy-saving and emission reduction enjoys popular support. People are longing for a higher quality of life while advocating a low-carbon way of life. Radiant cooling systems are favored by more and more people because of their performance of excellent comfort and energy-saving (Feng et al., 2013). Therefore, radiant cooling systems have also become the focus of study by experts and scholars in the HVAC field.

Radiant cooling/heating systems differ from traditional convective air-conditioning systems in that there exist a series of problems such as "air-conditioning diseases," air blows, and noise. The radiant cooling systems increase cooling areas and reduce the inner surface temperatures of envelopes, thus achieving the effect of energy-saving (Karmann et al., 2017; Hu and Niu, 2012). Taeyeon Kim (2001), Shuzo Murakami (2001), and Stetiu (1999) came to conclusion that the radiant cooling system had certain energy-saving advantages over traditional all-air systems through CFD simulation and energy consumption analysis, and pointed out when peak electricity was 27%, the former can save 30% of energy consumption compared to the latter.

* Corresponding author at: National Centre for International Research of Low-carbon and Green Buildings, Ministry of Science & Technology, Chongqing University, Chongqing 400045, China.
E-mail addresses: nanlicqu@126.com (N. Li), cq_505@163.com (Q. Chen).

https://doi.org/10.1016/j.ijrefrig.2019.10.016
0140-7007/

Nomenclature

A	area (m^2)
AUST	average unheated surface temperature (°C)
σ	Stefan–Boltzmann constant (W/m^2 K^4)
$F_{\varepsilon s\text{-}j}$	radiation interchange factor
$F_{s\text{-}j}$	view factor between radiant surface and j-surface
Q_{tot}	total heat flux (W)
q_{tot}	total heat flux density (W/m^2)
h_{tot}	total heat transfer coefficient (W/m^2 K)
Q_r	radiant heat flux (W)
q_r	radiant heat flux density (W/m^2)
h_r	radiant heat transfer coefficient (W/m^2 K)
Q_c	convective heat flux (W)
q_c	convective heat flux density (W/m^2)
h_c	convective heat transfer coefficient (W/m^2 K)
c_p	specific heat (J/kg K)
M	mass flow rate (kg/s)
T_a	air temperature (°C)
T_{op}	operative temperature (°C)
T_s	radiant surface temperature (°C)
T_{in}	the temperature of supply water (°C)
T_{out}	the temperature of return water (°C)
T_j	j-surface temperature (°C)
T_{ref}	reference temperature (°C)
$\triangle T_w$	the temperature difference between supply and return water (°C)
ε	Emissivity
λ	thermal conductivity (W/m K)
R	radius (m)
ϵ	surface tension (N/m)
α	heat transfer coefficient (W/m^2 K)
M	molar mass (kg/mol)
δ	the thickness of the liquid film (m)
δ_0	the thickness of the balanced liquid film (m)
h_{fg}	latent heat of vaporization (kg/kg)
R	gas constant (J/mol K)
V	molar volume (m^3/mol)
p	pressure (Pa)

Lower mark

c	capillary mat
i	interface
m	meniscus
v	vapor
w	wall surface
l	liquid

Supplying fresh air to bear the indoor wet load and partial cooling load is a great choice for solving the problem of condensation (Lim et al., 2006), radiant cooling/heating coupled with ventilation systems is called a hybrid system which can play an important role in improving energy efficiency and indoor thermal comfort at the same time (Song et al., 2008).

At present, researches on radiant cooling/heating systems mainly include the following aspects: (1) thermal comfort analysis (2) cooling capacity calculation (3) energy-saving analysis and (4) control strategy formulation. Such as Kilkis (1994) and Richard and Strand (2005, 2003) have made their meaningful contribution to the profound development of radiant cooling systems.

There are many previous pieces of research focusing on heat transfer coefficients of radiant panel systems. Feustel and Stetiu's (Feustel HE, 1995) test results on the cooling ceiling showed that the total, radiant and convective heat transfer coefficient were 9–12 W/m^2 K, 5.5 W/m^2 K, 3.5–5.5 W/m^2 K, respectively. Causone et al. (2009) used a heating cylinder and a cooling surface to simulate the inner heat gain in the room. The experimental data showed that the total and radiant heat transfer coefficients of the cooling ceiling were approximately 13.2 W/m^2 K and 5.8 W/m^2 K. Koca et al. (2014) conducted an experimental test on the radiant heating walls equipped in the climate test chamber. The results indicated that the average value of the radiant heat transfer coefficient was 5.7 W/m^2 K, and the convective heat transfer coefficient was about 2.7 W/ m^2 K. In the study of the ceiling cooling system, Rees and Haves (2013) found the radiant heat transfer coefficient of radiant and displacement ventilation systems was 5.9 W/m^2 K. Cholewa et al. (2013) thought that people overestimated the values of heat transfer coefficients of radiant systems in the previous researches. The value of heat transfer coefficient of the heating/cooling radiant floor was known after analyzing the experimental data, which was even 10%−30% higher than the actual value.

Corresponding experiments and simulations on displacement ventilation have been carried out in Japan and the United States in the early 1990s, and it had been commonly applied in Northern Europe since then (Xiaxiong Yuan and Glickman, 1998). The principle is that fresh air is delivered at the bottom of the room at a very low wind speed (0.03–0.2 m/s) with 2 to 4 °C temperature difference with the indoor air temperature (Skistad, 1996) and it was shown that the small movement of the indoor airflow helped to improve the thermal comfort of the air-conditioned environment (Koichi Kitagawa, 1999), of which the high efficiency have opened up a broad application prospect for it. Awbi (1998) and Xing (2001) reported that higher air quality can be obtained in the working area of the room with displacement ventilation compared with mixed ventilation by CFD simulation.

Obviously, the height of thermal stratification is an important design basis for displacement ventilation systems. Mundt (1995) established a mathematical model for calculating the vertical air temperature gradient in the room with displacement ventilation systems based on a large number of theoretical analysis. Xing (2002) conducted an experimental study of displacement ventilation systems whose thermal stratification height was affected by the amount of heat load.

In general, there are many research papers on thermal comfort, thermal analysis and system configuration and control of the RHC system in the last fifty years.

However, it is well known that the main disadvantage of the radiant system is lying on the long response time, so the research of the response performance is the basis of developing a better control strategy. Secondly, the capillary mat is increasingly popular in China. Different from the radiant panel which has been studied in much previous literature, the heat transfer characteristics of the capillary mat is not digged out completely. Finally, more and more hybrid systems are put into application for making up for the poor indoor fresh air quality by single radiant systems, so the regulation and management of the hybrid systems are supposed to be optimized.

In this paper, the response time of the capillary mat is measured and prepared for a better control strategy of radiant systems, which is supposed to be developed in the following research. then the heat transfer characteristic of the capillary mat is measured and compared with the other types of radiant terminals. It is worth noting that the capillary mat that is made up of thinner pipes similar to the human being's veins is different from conventional radiant panels, so the comparasion between this two is benefitial for judging whether it is worth using the capillary mat for better heat transfer performance sacrificing with the unflexibility of installation. Besideds, the influence of water supply temperature, air supply volume, air supply temperature on the indoor thermal com-

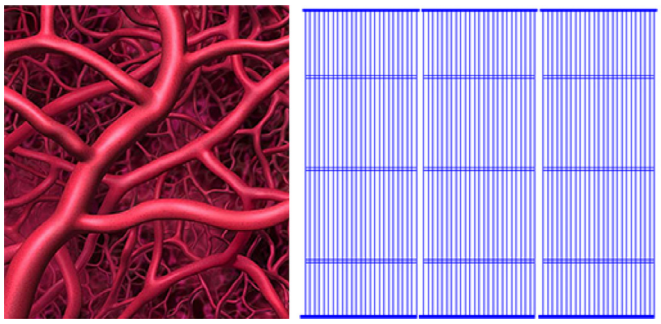

Fig. 1. Capillaries of human beings and Schema of capillary mat.

fort of radiant cooling coupled displacement ventilation systems is studied through orthogonal experiments, which can provide a reference for the regulation and management of hybrid systems.

2. Capillary mat radiant system

Capillary mat simulates the capillary mechanism of human veins, consisting of a cluster of capillaries with an outer diameter of 3.5–5.0 mm (wall thickness 0.9 mm) and a length of 1–6 m. The schema of the capillary mat of which the configuration is similar to the human being's veins is shown in Fig. 1 (Ren Jie and Jingming, 2008). Capillary mat has a larger cooling surface area than common air-conditioning systems and the supply water temperature is set at a relatively higher temperature of nearly 16~18 °C in order for energy efficiency (Kim Wufeng and Guangyu, 2010). On the one hand, the capillary mat has the characteristics of large heat exchange area, excellent thermal conductivity, uniform heat transfer, and small hydraulic loss, which contributes to energy efficiency, more comfortable indoor environment, reliving the power peak and so on (Ning et al., 2017). On the other hand, there are some problems such as high energy consumption and the strong feeling of blowing for conventional air-conditioning systems though their response is more rapid relatively. In summary, the advantages and disadvantages of the radiant cooling system and the conventional air-conditioning system are shown in Fig. 2.

At present, many researchers and scholars focus on the in-depth study of empirical correlations capillary tubes (Sarker and Jeong, 2012; Shao et al., 2013; Yang and Wang, 2008). Jinliang (1999) theoretically analyzed the heat transfer process in the capillary mat and proposed a calculation method for its heat transfer performance. An example calculation was also performed. The evaporation meniscuses inside capillary mat consist of the equilibrium thin-film zone, the transition film zone, and intrinsic meniscus zone. The calculation example showed that the diameter of the capillary mat had huge significance on the meniscus zone. The average heat transfer coefficient gradually decreases with the increase of the pipe diameter.

3. Experimental device

The experimental room is used for measurements to assess the dynamic heat transfer performance for three types of radiant capillary mat terminals coupled with ventilation systems.

The net internal dimensions of the experimental room for measurements are equal to 6 m × 5 m × 3.5 m; three walls of the room are surrounded by the adjacent rooms, which are not controlled but stable conditions. The ceiling and floor are separated from the precast concrete slabs by a 120mm-thick insulation board. The heat transfer coefficients for single-layer windows and doors are 6.4 W/m^2 K and 2.91 W/m^2 K, respectively.

The capillary mat water channel is composed of a random copolymer polypropylene pipe (*PP-R*) tube of which the diameter is 3–5 mm and wall thickness is about 0.5–0.8 mm. The surfaces are coated with a mortar and other materials and the allowable hot water temperature of the different capillary mat is generally between 45 °C–80 °C. Capillary mats are installed at the ceilings, walls, and floors in the environmental room for corresponding experiments. Detailed information of capillary mat is illustrated in Table 1. The detailed size is selected for different experimental rooms and the total areas of the capillary mat with the same tube spacing is presented in the table. The experiments were carried out in the typical months of July and August in hot-summer and cold-winter zones of China.

The ventilation system was turned on in order to prevent condensation during the experiments for heat transfer coefficients of the capillary mat. And the displacement system was on operation when experiments for performance research of hybrid systems were conducted.

The temperatures of the internal surfaces were measured in plum-shaped and indoor air were instrumented at the height of 1.1 m above the floor at four points symmetrically about the center of the room, and all measurements of temperature were finished by T-type thermocouples. Calorimeter came with two temperature measuring points and a flow measuring point, the temperature measuring points were installed in the supply and return water mains, flow measurement point was arranged in the backwater mains. The emissivity of the testing room can be acquired by measurements through an infrared thermal imaging camera and a T-type sensor and the follow-up calculation. The type, model, measurement range and accuracy of all the instruments in the experiments are shown in Table 2.

4. Calculation of the heat transfer coefficients

The total heat flux between the cooling ceiling and the experiment room is determined via the following equation:

$$q_{tot} = \frac{Q_{tot}}{A} = \frac{mc_p \Delta T_w}{A} - \frac{Q_{out}}{A} = \frac{mc_p (T_{out} - T_{in})}{A} - \frac{Q_{out}}{A} \quad (1)$$

Q_{out} is the heat flux between the cooling surface and the neighboring room, which can be ignored in this paper considering its little percentage on the total heat flux.

The total heat flux is the sum of the radiant and convective heat transfer (h_r and h_c) between the test room and the cooling surface. The choice of reference temperatures is a key link in the calculation of the heat transfer coefficients (Zhang et al., 2013). According to the previous literature, T_{op} can be used as a reference temperature for calculating the total heat transfer coefficient. Correspondingly, the average unheated surface temperature (AUST) and indoor air temperature (T_a), which is the air temperature at the height of 1.1 m, are used for calculation of radiant and convective heat transfer coefficients (h_r and h_c) as reference temperatures (T_{ref}).

$$h_{tot} = \frac{Q_{tot}/A}{T_{op} - T_s} \quad (2)$$

Radiant heat transfer coefficient (h_r) is associated with the radiant exchanged heat between the working surface and the non-working surfaces.

$$q_r = \frac{Q_r}{A} = \sigma \sum_{j=1}^{n} F_{\varepsilon_{s-j}} \left(T_s^4 - T_j^4\right) \quad (3)$$

The average indoor non-heated surface temperature (*AUST*) is the weighted average of the indoor surface temperatures, related to the view factors between the working and non-heated surfaces (ASHRAE, 2000; Watson and Chapman, 2002) which is obtained by checking the corresponding table according to the room size, and

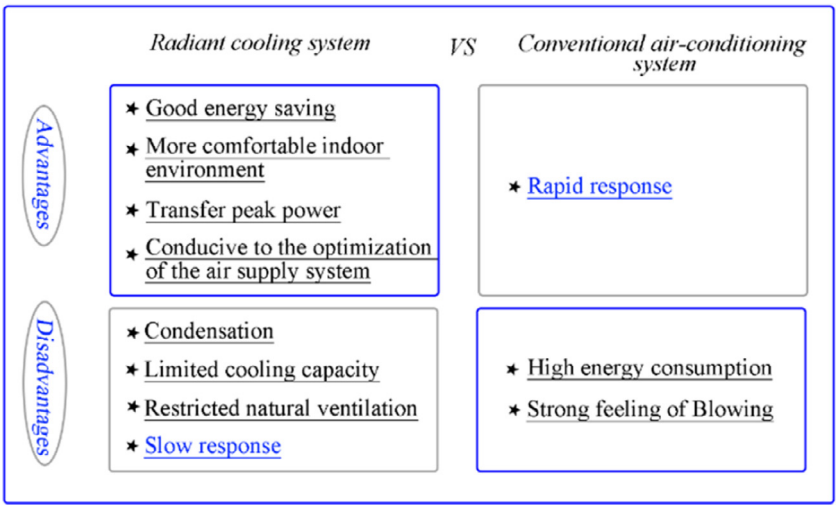

Fig. 2. The advantages and disadvantages of the radiant cooling system and the conventional air-conditioning system.

Table 1
Detailed information on capillary mat.

Terminals	Specification (mm × mm)	Quantity	Tube spacing (mm)	Area (m^2)	Total area (m^2)
Ceiling	1000 × 10,000	2	20	10	16
	600 × 10,000	2	20	6	
Wall (left)	1000 × 5000	5	20	12.5	25
Wall (right)	1000 × 5000	5	20	12.5	
Floor	1000 × 7000	3	20	10.5	10.5

Table 2
Specification of measurement instruments.

Instrument	Model	Range	Accuracy
Calorimeter	UH32-6.0	0 °C–105 °C	± 0.01 °C
		0.02 m^3/h–2.0m^3/h	± 0.001 m^3/h
		/	± 1kW h
T-type thermal couple	/	−40~+125 °C	±0.5 °C
Agilent data collection meter	Agilent 34970A	−200~+350 °C/	/
HOBO Temperature and humidity recorder	HOBO/UX100-011	temperature:−20 °C–70 °C	temperature:±0.21 °C
		relative humidity:1%–95% RH	relative humidity:±3.5% (25%–85%) , ± 2.5% (10%–90%)
anemograph	Swema 3000	0.1–30 m/s	0.10–1.33 m/s: ± 0.04 m/s
			1.33–30 m/s:± 3%measurement
Universal anemometer	AirDistSys 5000	0.05–30 m/s	0.02 m/s
		−20 °C–80 °C	±1% of measurement
Thermal imager	FLIR T650sc	−40 °C–150 °C	1% of the measurement

it is commonly used for the calculation of the radiant heat transfer coefficient as the reference temperature.

$$h_r = \frac{Q_r/A}{AUST - T_s} \tag{4}$$

$$AUST = \sqrt[4]{\sum_{j=1}^{n}\left(F_{s-j}T_j^4\right)} \tag{5}$$

$$F_{\varepsilon_{s-j}} = \frac{1}{[(1-\varepsilon_s)/\varepsilon_s] + \left(1/F_{s-j}\right) + \left(A_s/A_j\right)\left[\left(1-\varepsilon_j\right)/\varepsilon_j\right]} \tag{6}$$

The view factors of each surface (F_{s-j}) are obtained by checking the figure characterizing the relationship between geometry sizes and view factors, which is assumed as a constant value for a certain pair of the wall surface. And then radiation interchange factors ($F_{\varepsilon s-j}$) can be calculated according to Eq. (6).

The calculation of the convective heat transfer coefficient (h_c) is based on the convective heat transferred from the cooling surface to the room. The convective heat flux equals the total heat flux minus the radiant heat flux calculated by Eq. (7).

$$q_c = q_{tot} - q_r \tag{7}$$

$$h_c = \frac{Q_c/A}{T_a - T_s} \tag{8}$$

$$\omega_{q_r} = \frac{\left[\left(\frac{\partial q_r}{\partial T_s}\right)^2 + \sum_{j=1}^{n}\left(\frac{\partial q_r}{\partial T_j}\right)^2\right]^{\frac{1}{2}}}{q_r} \times 100 \tag{9}$$

$$\omega_{q_c} = \frac{\left[\left(\frac{\partial q_c}{\partial Q_{tot}}\right)^2 + \left(\frac{\partial q_c}{\partial q_r}\right)^2\right]^{\frac{1}{2}}}{q_c} \times 100 \tag{10}$$

$$\omega_{h_r} = \frac{\left[\left(\frac{\partial h_r}{\partial T_s}\right)^2 + \sum_{j=1}^{n}\left(\frac{\partial h_r}{\partial T_j}\right)^2\right]^{\frac{1}{2}}}{h_r} \times 100 \tag{11}$$

$$\omega_{h_c} = \frac{\left[\left(\frac{\partial h_c}{\partial Q_c}\right)^2 + \left(\frac{\partial h_c}{\partial T_a}\right)^2 + \left(\frac{\partial h_c}{\partial T_s}\right)^2\right]^{\frac{1}{2}}}{h_c} \times 100 \tag{12}$$

In the experiment, the uncertainty is inevitable from the experimental apparatus and people's inappropriate operation, which

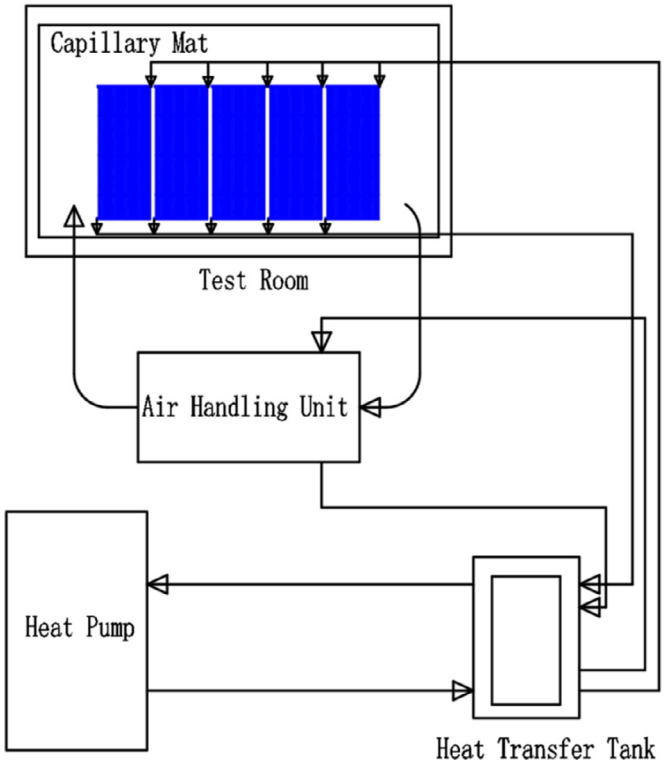

Fig. 3. Schema diagram of the experimental system.

is likely to result in relative errors. Therefore, the uncertainty values are calculated according to Eq. (9)–(12) (Babayigit et al., 2017). The accuracy values of measurement equipment are seen in Table 2. The uncertainty values of q_r, q_c, h_r, h_c are found to be less than ±2%.

5. Experimental procedure

The experiments were conducted in Chongqing province in China. The schema diagram of the experimental system is shown in Fig. 3. The entire cooling system is powered by a heat pump, and the secondary side cold water and the outlet water of the heat pump exchange heat through the heat exchange water tank, wherein the air from the air handling unit is also cooled. In cool conditions, the water supply temperatures (T_{in}) were set as follows: 16 °C, 18 °C, and 20 °C, because condensation occurred when the temperature of supply water was set at 14 °C.

The air supply volumes were set to be equivalent to 100 m^3/h (1 time/h), 200 m^3/h (2 times/h) and 300 m^3/h (3 times/h). The air supply speeds were 0.27 m/s for displacement ventilation. The schema diagram of the ventilation system is shown in Fig. 4 where the mixed ventilation system, the orifice ventilation, and the displacement ventilation system can be switched as needed with different supplying vents. The air supply temperatures (T_a) were set at 23 °C, 24.5 °C and 26 °C for displacement ventilation. The experimental case arrangements are shown in Table 3, and the experiment is divided into three parts. In the first part, the performance between the ceiling, floor, wall cooling at different water supply temperatures is compared. In the second part, the performance of the ceiling cooling under different air supply volumes is compared. In the third part, the orthogonal experiment is carried out to study the influence of water supply temperature, air supply volume and air supply temperature on the ceiling cooling coupled displacement ventilation system.

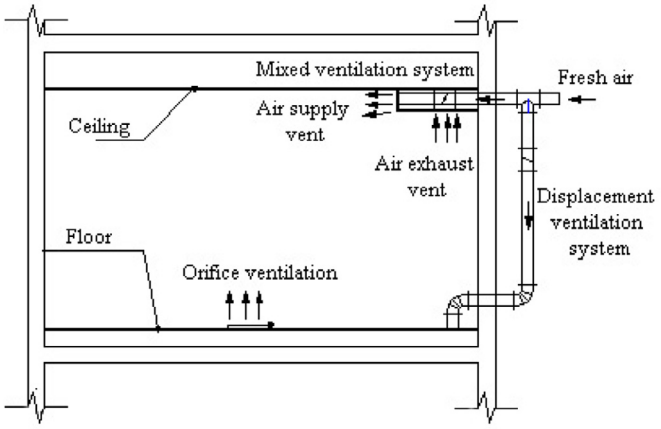

Fig. 4. Schema diagram of the ventilation systems.

Table 3
The experimental case arrangements.

Location of capillary mat	Water supply temperature (°C)	Air supply volumes (m^3/h)	Air supply temperature (°C)
Ceiling	16	100	–
	18	100	
	20	100	
Wall	16	100	
	18	100	
	20	100	
Floor	16	100	
	18	100	
	20	100	
Ceiling	16	200	
	18	200	
	20	200	
Ceiling	16	300	
	18	300	
	20	300	
Ceiling+Displacement ventilation	16	100	23
	18	200	23
	20	300	23
	16	200	24.5
	18	300	24.5
	20	100	24.5
	16	300	26
	18	100	26
	20	200	26

All measurements were recorded in real-time by the Agilent Data Logger and archived in 5-min time steps. The analysis of heat transfer coefficients is based on experiment data during the steady state. About 8 h after the system was shut down, the surface temperature of the envelopes can be restored to within a range of 24 h before, which meant that the thermal inertia of the envelope did not affect the experimental results.

6. Results and discussion

6.1. Response time

The indoor air temperature (T_a) under ceiling, wall and floor cooling is shown in Fig. 4. For the radiant ceiling cooling, the response time of the indoor air temperature (T_a) is analyzed at water supply temperatures (T_{in}) of 16 °C, 18 °C, and 20 °C.

It can be seen from Fig. 4(a) that the indoor air temperature (T_a) decreased significantly within 1hr under three working conditions, and the indoor air temperature (T_a) was reduced the fastest at this time. After that, the indoor air temperature (T_a) stayed stable nearly, showing a steady decline due to the influence of solar radiation and the load of the enclosure. Within 5 h after shut-

Table 4
The indoor air temperature drop rates in the initiating and attenuation stages.

Location	Temperature change rate	16 °C	18 °C	20 °C
Ceiling	Initiating stage	2.44	1.8	1.42
	Attenuation stage	0.52	0.36	0.31
Wall	Initiating stage	1.11	0.76	0.69
	Attenuation stage	0.22	0.16	0.22
Floor	Initiating stage	0.58	0.49	0.29
	Attenuation stage	0.32	0.31	0.26

down (23:00), the indoor air temperature (T_a) increased at a higher rate, and then remained substantially stable. As the water supply temperature (T_{in}) decreased, the response time of the indoor air temperature (T_a) was significantly reduced.

Here, the indoor air temperatures (T_a) at the initiating stage (8:00–9:00) and the attenuation stage (23:00–7:00) are mainly analyzed.

In the initiating phase, the temperature drop rate was the fastest when the water supply temperature (T_{in}) was 16 °C, and the indoor air temperature (T_a) reached 27 °C when the system was running for about 35 min. Under the condition that the water supply temperature (T_{in}) was 20 °C, the indoor air temperature (T_a) reached 28 °C after the system was running for 15 min, and then it has remained stable since and there was no obvious downward trend due to the limited cooling capacity of the system, which showed that in the summer for the radiant ceiling cooling, the lower water supply temperature can effectively increase the temperature drop speed and can help to achieve demanded indoor environment faster. Moreover, the water supply temperature (T_{in}) of 20 °C is difficult to meet the comfort requirements of the room in the case where the outdoor temperature is relatively high (outdoor average dry bulb temperature is higher than 34.0 °C).

During the initiating stage, the temperature drop rate was increased by about 0.27 times when the water supply temperature (T_{in}) was lowered from 20 °C to 18 °C. while the water supply temperature (T_{in}) was lowered from 18 °C to 16 °C, and the temperature drop rate was increased by about 0.36 times.

It can be seen from Fig. 5(b) that the indoor air temperature (T_a) dropped significantly within 2 h from starting under three working conditions. At this time the drop rate of the indoor air temperature (T_a) was the largest. Then, the indoor air temperature (T_a) showed a steady-decline trend in the stable phase. Within 5 h after shutdown (23:00), the indoor air temperature (T_a) increased at a relatively high rate before keep basically stable.

It can be seen from Table 4 and Fig. 5(b) that in the start-up phase, the indoor air temperature (T_a) dropped the fastest while the water supply temperature was 16 °C and reached 27 °C when the system was running for about 80 min. When the water supply temperature (T_{in}) was 18 °C, it took 20 min for the indoor air temperature (T_a) to reach 28 °C, after which the indoor air temperature slowly decreased and reached the set temperature of 27 °C after running 12.6 h. At 20 °C, the indoor air temperature dropped to 28 °C after about 9 h and was always above the set temperature of 27 °C.

During the initiating stage, the temperature drop rate was increased by about 0.11 times when the water supply temperature (T_{in}) was lowered from 20 °C to 18 °C. while the water supply temperature was lowered from 18 °C to 16 °C, and the temperature drop rate was increased by about 0.46 times.

It can be seen from Fig. 5(c) that, the indoor air temperature (T_a) cut down significantly within 2 h from starting under three working conditions and changed little from 9:00 to 16:00 before there was a significant drop after 16:00. Afterward, the indoor air temperature increased within 5 h after shutdown (23:00) and then remained generally stable.

In the initiating stage, there were about 20 min before the indoor air temperature (T_a) reached 27 °C when the water supply temperature was 16 °C, followed by 50 min for 18 °C water supply temperature and 14 h for 20 °C water supply temperature. During this stage, the temperature drop rate was increased by about 0.68 times when the water supply temperature (T_{in}) was lowered from 20 °C to 18 °C. while the water supply temperature was lowered from 18 °C to 16 °C, and the temperature drop rate was increased by about 0.18 times.

During the attenuation phase, the indoor air temperature (T_a) experienced a faster decay within 5 h after the system was shut down and finally tent to be flat. And compared with Table 4, it can be found that the rising rate of the indoor air temperature tent to increase as the water supply temperature decreased.

6.2. The cooling capacity

The cooling water temperature, indoor air temperature, surface temperature and the calculated parameters such as AUST, radiant, convective and total heat flux are shown in Table 5.

According to the results in Table 5, it can be seen that the calculated heat transfer coefficient of the capillary mat shows a slight difference compared with the previous researches, slightly higher than that actually used. More detailed analysis of heat transfer coefficients and cooling capacity are illustrated as followed.

6.2.1. Heat transfer coefficient

The radiant heat transfer coefficients (h_r) given by former researchers and this study are shown in Fig. 6(a). As seen in Fig. 6(a), radiant heat transfer coefficients are supposed to be a constant, which comes to an agreement with previous studies.

This result can be reasonably explained by observing Eqs. (3–4): radiant heat transfer coefficient (h_r) is related to the following factors: the Stefan–Boltzmann constant, the emission rate of each interior surfaces, the angular coefficient, and the inner surface temperatures. For a given building, the emissivity and the angular coefficients of the interior surfaces can be considered as constant. Therefore, the radiant heat transfer coefficient is only depending on inner surface temperatures (Rhee and Kim, 2015). However, their impacts on the linear radiant heat transfer coefficients are limited due to the relatively low surface temperatures in the room and small variation range.

Fig. 6(b) shows the convective heat transfer coefficients (h_c) for different water supply temperatures (T_{in}) and ventilation frequency. Convective heat transfer coefficient is related to air temperature, turbulent boundary layer, airflow organization and, air velocity so on (Zhao et al., 2016). It can be seen that the convective heat transfer coefficient ranges from 3.45 to 4.00 W/m^2 K.

The data comparison result of the three groups of experiments is shown in Table 6, verifying whether the two groups of data in the comparison can share a common linear equation. It is not difficult to find that there is a small probability of error in sharing a linear equation among the three data sets, which are respectively 2.45×10^{-4}, 1.84×10^{-13}, and 8.66×10^{-9}, this also proves from the side that radiant heat transfer coefficients obtained in this paper and previous results are exceedingly close.

The total heat transfer coefficient (h_{tot}) expounds the comprehensive reflection of radiant and convective heat transfers (h_r and h_c), but a simple superposition of the two heat transfer coefficients cannot generate a scientific value apparently. Therefore, there is no detailed discussion of the total heat transfer coefficient.

6.2.2. Heat flux density

The cooling water temperature, the surface and indoor air temperatures, the radiant, convective and total heat flux for capillary mat ceiling, wall and floor are shown in Table 7.

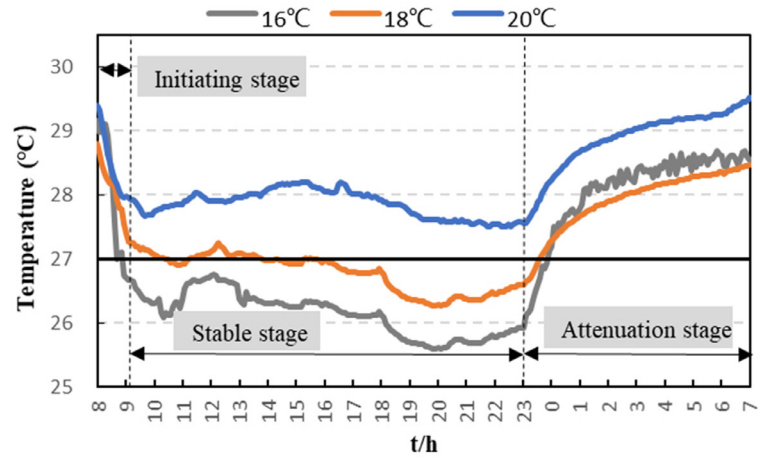

(a) The ceiling

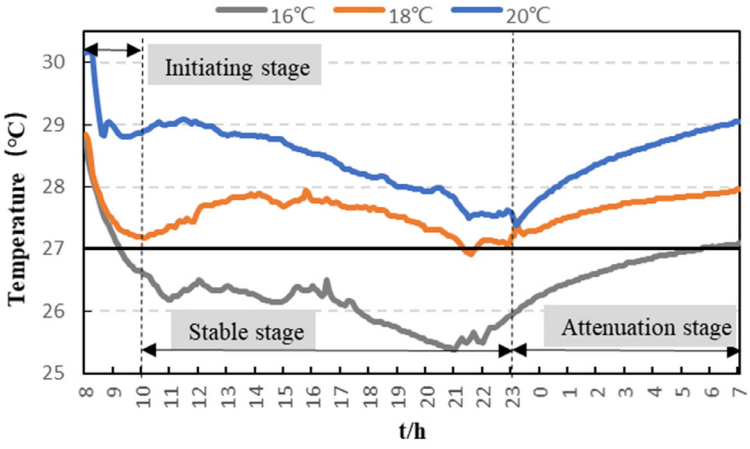

(b) The wall

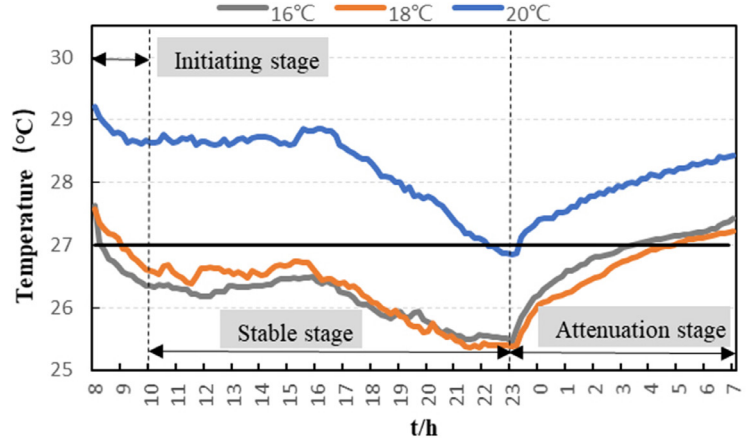

(c) The floor

Fig. 5. The indoor air temperature.

Radiant and convective heat flux densities (q_r and q_c) of the cooling ceiling are presented in Fig. 7(a) when the ventilation frequency (n) equals to 1 time/h, 2 times/h and 3 times/h. The total heat flux increased by nearly15%–20% for cooling ceilings when the water supply temperature (T_{in}) decreased from 20 °C to 16 °C. When the ventilation frequency was 1 time/h, the total heat flux density (q_{tot}) decreased with the water supply temperature increasing, but the proportion of radiant heat flux density on the total heat flux density was nearly constant, which also applied to the other two cases (ventilation frequency is 2 times/h or 3 times/h).

Table 5
Measured and calculated parameters for the capillary mat ceiling system.

case	1	2	3	4	5	6	7	8	9
n(/h)	1	1	1	2	2	2	3	3	3
T_{in}(°C)	16.00	18.00	20.00	16.00	18.00	20.00	16.00	18.00	20.00
T_{in}'(°C)	16.30	17.94	19.42	15.71	17.68	19.64	15.84	17.67	19.36
T_{out}'(°C)	19.56	20.81	21.91	19.01	20.46	22.02	19.96	21.42	22.62
T_s(°C)	18.90	20.68	21.66	19.06	20.21	21.23	19.96	20.82	21.62
T_a(°C)	26.40	27.00	28.00	25.78	25.92	26.98	26.43	26.84	26.35
AUST(°C)	28.48	27.28	28.09	26.25	26.62	27.79	27.60	27.32	28.39
q_{tot}(W/m²)	74.3	62.7	61.8	67.8	58.2	59.3	68.5	59.9	55.2
q_r(W/m²)	44.3	38.4	37.4	41.9	37.4	38.2	43.9	37.6	38.9
h_r(W/m² K)	5.84	5.82	5.82	5.83	5.83	5.82	5.75	5.78	5.75
q_c(W/m²)	30.0	24.3	24.4	25.8	20.9	21.1	24.6	22.4	16.3
h_c(W/m² K)	4.00	3.84	3.85	3.85	3.66	3.66	3.80	3.72	3.45

Table 6
Results of linear regression analysis.

Case1	Case2	F	Numer.DF	Denom.DF	Prob > F
This study	Causone	16.85	2	13	2.45×10^{-4}
This study	Cholewa	585.24412	2	13	1.84×10^{-13}
Causone	Cholewa	126.40067	2	12	8.66×10^{-9}

So, it can be concluded that the proportion of radiant heat transfer on the total heat transfer for the cooling ceiling distributes from 60%−70% with natural ventilation.

Radiant and convective heat flux densities (q_r and q_c) for three types of capillary mat terminals are presented in Fig. 7(b) when the water supply temperature (T_{in}) is 16 °C, 18 °C, 20 °C, respectively. It can be seen that the cooling capacity of the ceiling was the best and that of the floor was lower than other types apparently. The total heat flux (q_{tot}) decreased by about 8%−15% when the water supply temperature increased from 16 °C to 18 °C. When the water supply temperature (T_{in}) increased from 18 °C to 20 °C, the total heat flux experienced a decrease of about 1%−10%. The water supply temperature had a more significant impact on the floor which can be illustrated by approximately 30% increase of heat flux when the water supply temperature dropped from 20 °C to 16 °C. The proportion of radiant heat flux density (q_r) on the total heat flux density (q_{tot}) for ceiling and wall was about 60%−64%. However, the proportion of radiant heat flux on the total heat flux for the floor was higher than that of other types, which was about 80%. This was because that cooled air dropped around the floor harmful to convective heat transfer between the cooling floor and the indoor air.

As seen in Table 7, the ratios of radiant flux to the total heat flux for meandering type and spiral type of radiant panel are nearly 57%– 61% and, respectively, on the cooling condition according to 'Okamoto et al. (2010) research, and that of Koca et al.'s research is about 67%−70%, which is close to that of the capillary mat and verifies the small difference of heat transfer characteristic of variant types of radiant terminals.

Table 8
Indoor thermal index for 9 cases.

Case	PMV	PPD	$t_{1.1}-t_{0.1}$/°C	$t_{1.7}-t_{0.1}$/°C
1	0.32	7.17	0.64	0.85
2	0.18	5.64	0.80	1.07
3	0.39	8.09	1.57	1.95
4	0.16	5.50	0.78	0.78
5	0.42	8.61	1.39	1.39
6	0.92	22.87	0.81	1.11
7	0.367	7.80	1.22	1.37
8	0.431	8.87	0.69	0.94
9	0.576	11.95	1.04	1.10

PMV-PPD:thermal comfort evaluation index based on air temperature, humidity, indoor airspeed, ambient radiation temperature, body metabolism and thermal resistance of clothes.
$t_{1.7}$-the indoor temperature in the height of the head when the human body stands.
$t_{1.1}$-the indoor temperature in the height of the head when the human body sits down.
$t_{0.1}$- the indoor temperature in the height of the human ankle.

6.3. Orthogonal experimental results

Orthogonal experiments were used to comprehensively investigate the influence of various factors including air supply temperature, water supply temperature, and air supply volume on the indoor thermal environment. There are several thermal comfort indexes such as PMV, PPD, $t_{1.1}-t_{0.1}$, $t_{1.7}-t_{0.1}$ presented in Table 8. In order to ensure the thermal comfort of working areas, there are specific requirements as follows: $-0.5<PMV<0.5$, $PPD<10\%$, $t_{1.1}-t_{0.1}<2.0$ °C and $t_{1.7}-t_{0.1}<3.0$ °C. $t_{1.1}-t_{0.1}$ represents the vertical air temperature difference between the top of the head and the ankle when the human body sits down. $t_{1.7}-t_{0.1}$ represents the vertical air temperature difference between the top of the head and the ankle when the human body is standing.

Table 7
Measured and calculated parameters for the capillary mat ceiling, wall, and floor.

Case	1	2	3	10	11	12	13	14	15
Type	ceiling			wall			floor		
T_{in}(°C)	16.00	18.00	20.00	16.00	18.00	20.00	16.00	18.00	20.00
T_s(°C)	18.90	20.68	21.66	19.40	20.20	22.30	20.40	21.70	24.10
T_a(°C)	26.40	27.00	28.00	26.40	27.90	28.60	26.60	26.50	28.90
q_{tot} (W/m²)	74.3	62.7	61.8	63.5	58.4	57.1	42.3	35.8	32.4
q_r (W/m²)	44.3	38.4	37.4	40.2	36.1	36.6	33.9	28.6	26.3
q_c (W/m²)	30.0	24.3	24.4	23.3	22.3	20.5	8.4	7.2	6.1

Case	Radiant terminal	Radiant flux ratio	Convective flux ratio
This study	capillary mat	60%−64%	36%−40%
Okamoto et al.	radiant panel (spiral and meandering)	57%−61%	39%−43%
Koca et al.	radiant panel	64%−71%	29%−36%

Table 9
Results of intuitive analysis for $t_{1.1}-t_{0.1}$ and $t_{1.7}-t_{0.1}$.

Case	$t_{1.1}-t_{0.1}$					$t_{1.7}-t_{0.1}$				
	Air supply temperature (A) (°C)	Water supply temperature (B) (°C)	Air supply volume (C) (/h)	Y_i	$(Y_i)^2$	Air supply temperature (A) (°C)	Water supply temperature (B) (°C)	Air supply volume (C) (/h)	Y_i	$(Y_i)^2$
1	23	16	1	0.64	0.41	23	16	1	0.85	0.72
2	23	18	2	0.80	0.64	23	18	2	1.07	1.14
3	23	20	3	1.57	2.46	23	20	3	1.95	3.80
4	24.5	16	2	0.78	0.61	24.5	16	2	0.78	0.61
5	24.5	18	3	1.39	1.93	24.5	18	3	1.39	1.93
6	24.5	20	1	0.81	0.66	24.5	20	1	1.11	1.23
7	26	16	3	1.22	1.49	26	16	3	1.37	1.88
8	26	18	1	0.69	0.48	26	18	1	0.94	0.88
9	26	20	2	1.04	1.08	26	20	2	1.10	1.21
K_1	3.01	2.64	2.14	$K=\Sigma Yi$	$W=\Sigma(Y_i)^2$	3.87	3.00	2.90	$K=\Sigma Yi$	$W=\Sigma(Y_i)^2$
K_2	2.98	2.88	2.62			3.28	3.40	2.95		
K_3	2.95	3.42	4.18			3.41	4.16	4.71		
R	0.06	0.78	2.04	8.94	9.76	0.59	1.16	1.81	10.56	13.41

As seen in Table 8, the indoor thermal environment under operating conditions satisfied thermal comfort requirements except for cases 6 and 9. Then, select the point near the heat source to further analyze the airflow in the experiment room.

As can be seen from Fig. 8, the heat/ mass transfer phenomena, the thermal comfort chart, and the indoor vertical air temperature are presented (Roshan et al., 2017). The thermal stratification heights for cases 1, 2 and 3 were basically maintained at approximately 0.9 m, 1.4 m, and 1.7 m, respectively. The thermal stratification heights for cases 4 and 5 were basically maintained at about 1.1 m and about 1.4 m, respectively. This was because the ceiling with a low water supply temperature (T_{in}) causes the sinking of the cold air, which in turn had a great influence on the airflow organization of the displacement ventilation.

The thermal stratification heights for cases 7, 8 and 9 were basically maintained at around 1.3 m, 0.9 m, 1.5 m, respectively. Although the cold load of case 7 was greater than that of case 9, the thermal stratification height was less than case 9, which indicated that the ceiling cooling weakened the temperature distribution resulting by the displacement ventilation. Therefore, the convective heat transfer should be minimized in a hybrid air-conditioning system. Under the premise of satisfying the environmental comfort, the higher water supply temperature (T_{in}) can weaken the cooling effect on the indoor air caused by the convective heat exchange, and also the lower energy consumption can be achieved. Therefore, in the design of the hybrid system combined cooling ceiling and displacement ventilation, selecting parameters of cooling ceiling and displacement ventilation carefully has much influence on energy-saving and comfortable flow field of indoor air.

Taking $t_{1.1}-t_{0.1}$, $t_{1.7}-t_{0.1}$ and indoor air temperature drop rate as evaluation indicators, it is proposed to optimize parameters of the hybrid system through visual analysis and analysis of variance.

Results of influence of air supply temperature (*A*), water supply temperature (*B*) and air supply volume (*C*) on $t_{1.1}-t_{0.1}$, $t_{1.7}-t_{0.1}$ and indoor air temperature drop rate by visual analysis and variance analysis are showed in Tables 9 and 10 and Fig. 9. The whole process of calculating *R* and *F* is presented in detail in the table, where *R* and *F* represent the influence degree of three factors on the performance of the ceiling cooling coupled displacement ventilation system, which will be explained in detail later. For variance analysis, we can obtain that $F_{0.95}$ (2, 2) = =19.00, $F_{0.90}$ (2, 2) = =9.00 by looking up tables.

It can be seen from Fig. 9 that under cooling conditions, the factors affecting $t_{1.1}-t_{0.1}$ and $t_{1.7}-t_{0.1}$ were ranked in order: air supply volume (*C*), water supply temperature (*B*), and air supply temperature (*A*) by visual analysis.

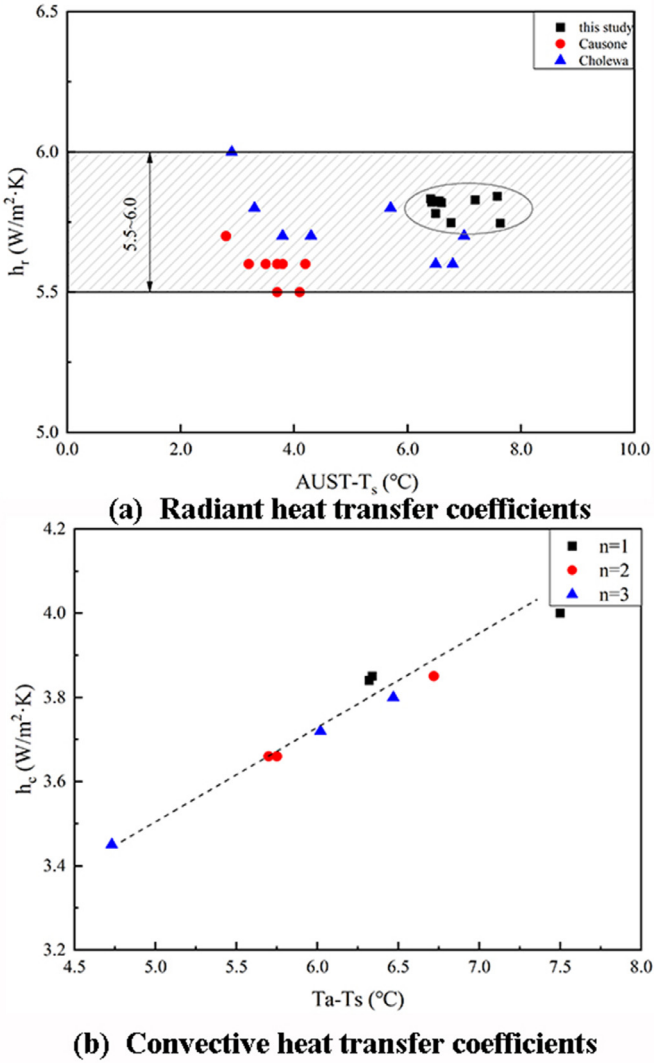

Fig. 6. Heat transfer coefficients for the cooling ceiling.

Due to the fact that $F_C = 66.53 > 19.00$ and $F_B = 9.33 > 9.00$ and $F_C = 38.09 > 19.00$ and $F_B = 12.44 > 9.00$, it can be concluded that the impact of air supply volume on $t_{1.1}$-$t_{0.1}$ and $t_{1.7}$-$t_{0.1}$ were significant in the case of the confidence level of 0.95. The water supply temperature (T_{in}) had a significant effect on $t_{1.1}$-$t_{0.1}$ and $t_{1.7}$-$t_{0.1}$ in

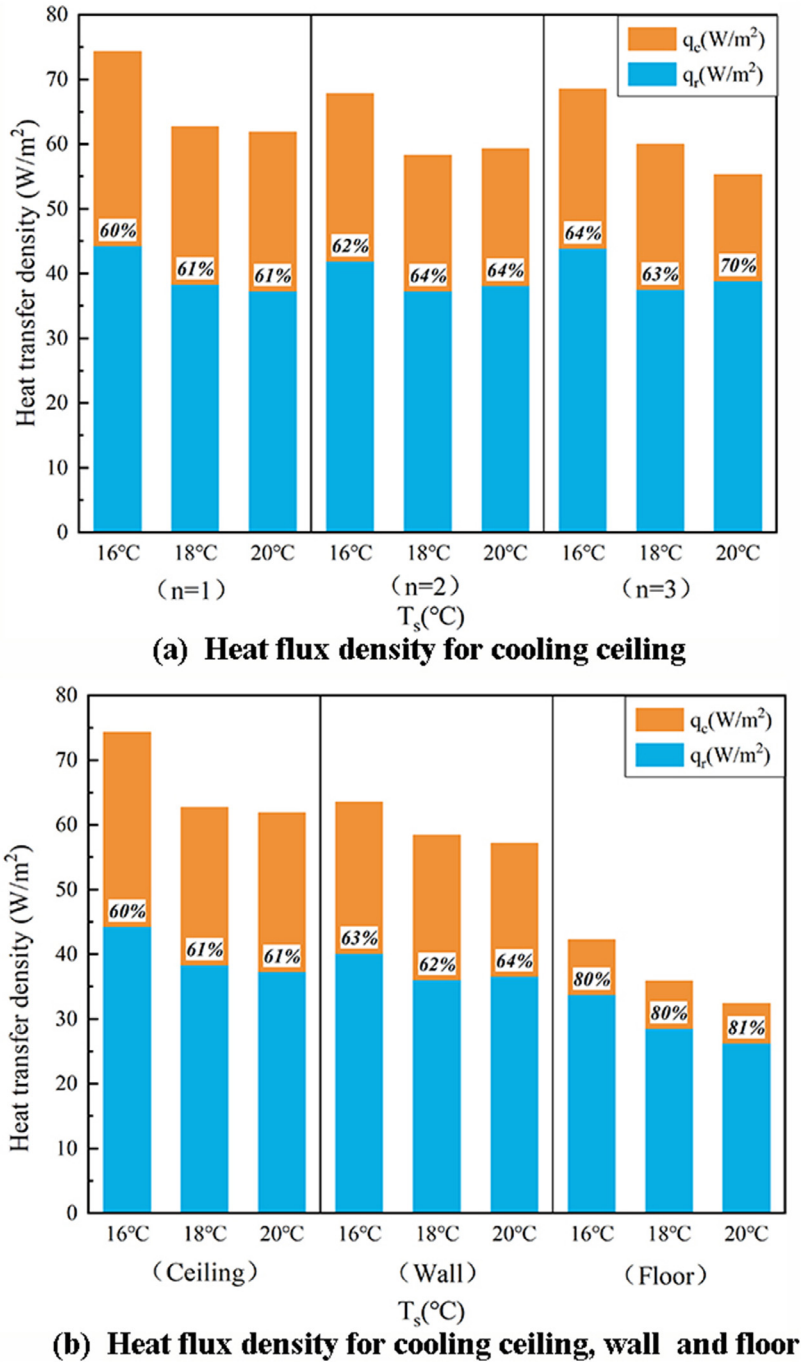

Fig. 7. Heat flux density.

the case of a confidence level of 0.90. But the effect of air supply temperature was negligible.

In cool conditions, the above two methods of data analysis all indicated that the air supply volume (C) and the water supply temperature (B) had a significant effect on $t_{1.1}-t_{0.1}$ and $t_{1.7}-t_{0.1}$, and the impact of the air supply volume (C) was more significant.

It can be seen that under cooling conditions, the factors affecting indoor temperature drop rate were ranked in order: water supply temperature (B), air supply volume (C), and air supply temperature (A) by institute analysis.

Due to the fact that $F_C = 10.16 > 9.00$ and $F_B = 37.95 > 19.00$, it can be concluded that the impact of water supply temperature on indoor temperature drop rate was significant in the case of the confidence level of 0.95. The air supply volume had a significant effect on indoor temperature drop rate in the case of a confidence level of 0.90. The air supply temperature had little influence on indoor temperature drop rate.

In cool conditions, the two methods of data analysis all indicated that the water supply temperature (B) and the air supply volume had a significant effect on indoor temperature drop rate, and the water supply temperature (B) has the most significant effect.

Taking the effects of thermal stratification height into account, indoor temperature drop rate, $t_{1.1}-t_{0.1}$, and $t_{1.7}-t_{0.1}$, it was found that the effect of factor A was not significant. That was, the air supply temperature can be considered as a secondary factor that

Table 10
Results of variance analysis for $t_{1.1}-t_{0.1}$ and $t_{1.7}-t_{0.1}$.

Factor	$t_{1.1}-t_{0.1}$				$t_{1.7}-t_{0.1}$			
	Q_x	f	S_x^2	F_x	Q_x	f	S_x^2	F_x
Air supply temperature (A)	0.06	2	0.03	3.44	0.16	2	0.08	5.26
Water supply temperature (B)	0.23	2	0.12	12.44	1.14	2	0.57	37.95
Air supply volume (C)	0.71	2	0.35	38.09	0.3	2	0.15	10.16
Q_E	0.02	2	0.01		0.03	2	0.01	
Q_T	1.02	8			1.63	8		

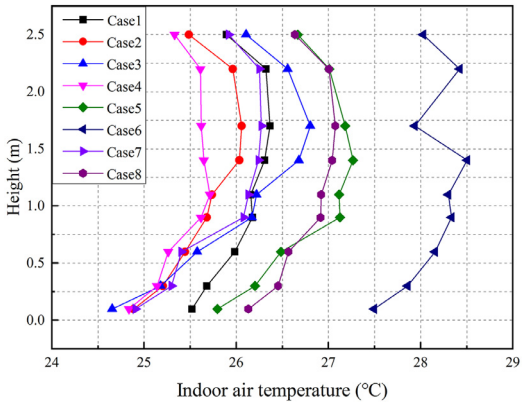

Fig. 8. The heat/ mass transfer phenomena, the thermal comfort chart, and the indoor vertical air temperature.

influenced the results of the experimental evaluation. Factors *B* and *C* had a significant effect.

When a higher air supply temperature is applied to the dew-point air supply system, the relative humidity of the air supply will be higher. Therefore, under the premise of satisfying the indoor thermal comfort, a lower air supply temperature should be preferred for displacement ventilation. On the one hand, the fresh air can be in charge of part of the indoor cooling load, so that a relatively high water supply temperature for ceiling can be used. On the other hand, it also avoids the increased energy consumption of reheating the air. A lower air temperature of 23 °C for displacement ventilation should be selected in summary.

Based on the analysis of the above evaluation indicators, it can be found that increasing the air supply volume can significantly increase the indoor temperature drop rate and the thermal stratification height, but air supply volume of 3 times/h obviously causes the higher energy consumption of fresh air, and air supply volume of 2 times/h can already ensure that the thermal stratification height is above the head of the human (the height of the head is 1.1 m when sitting).

Decreasing the water supply temperature helps to increase the indoor temperature drop rate, but the thermal stratification height will descend as a result. Comparing cases 2 and 4, it can be found that when the air supply volume is 2 times/h and the water supply temperature was 16 °C, it took 25 min for the indoor air temperature to reach 27 °C. And 35 min was needed before the indoor temperature was to 27 °C when the water supply temperature was 18 °C, which had no apparent advantage over the former case. Considering the indoor thermal environment and energy consumption comprehensively the water supply temperature of 18 °C is the optimal choice.

The optimum setting parameters can be obtained as follows: air supply temperature (*A*) 23 °C, water supply temperature (*B*) 18 °C, air supply volume (*C*) 2 times/h.

7. Conclusion

In this paper, experimental research was conducted for characterizing the dynamic heat transfer and cooling capacity performance of capillary mat and optimization of the hybrid system composing of radiant cooling and displacement ventilation. The response time is studied and can provide a reference for the proposal of the capillary mat. The obtained outcomes confirmed radiant heat transfer coefficients (h_r) reported in previous studies. The significance analysis results showed that the system parameters affecting the performance of the hybrid system are mainly the water supply temperature (T_{in}) and air supply volume, and the influence of the supply air temperature is small.

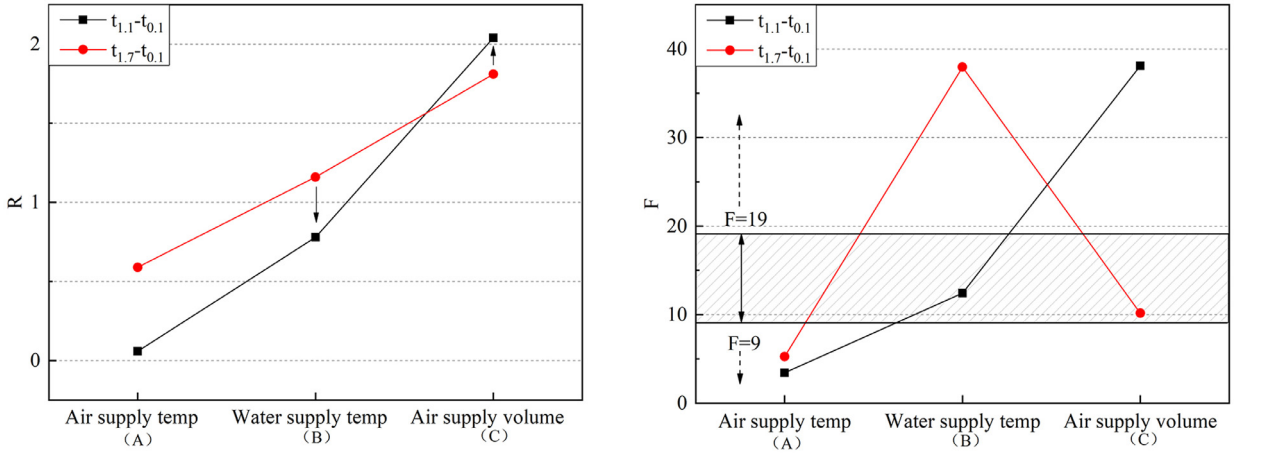

(a) Results of intuitive analysis for $t_{1.1}$-$t_{0.1}$ and $t_{1.7}$-$t_{0.1}$ **(b) Results of variance analysis for $t_{1.1}$-$t_{0.1}$ and $t_{1.7}$-$t_{0.1}$**

Fig. 9. Results of intuitive analysis and variance analysis for $t_{1.1}-t_{0.1}$ and $t_{1.7}-t_{0.1}$.

The indoor air temperature drop rates of the ceiling, wall and floor cooling are 1.42–2.44 °C/h, 0.69–1.11 °C/h, 0.29–0.58 °C/h in the response phase, which can provide reference for predictive control strategy in order to adapt to the thermal inertia of the radiant system.

For cooling capillary mat, radiant heat transfer coefficient of about 5.8 W/m^2 K can be recognized as a constant, close to the value of previous researches, which is 5.5–5.6 W/m^2 K. Convective heat transfer coefficients (h_c) are diverse from 3.45 to 4.00 W/m^2 K.

The total heat flux (q_{tot}) can experience an increase of 10%–30% when the water supply temperature (T_{in}) dropped from 20 °C to 16 °C. The cooling capacity for cooling ceilings is the largest and that of cooling walls is 7%–17% lower than that of cooling ceilings, the cooling capacity of cooling floors is 50%–76% lower than that of cooling walls and 75%–90% lower than that of cooling ceilings.

The proportion of radiant heat transfer on total heat transfer ranged from 60%–70% for cooling ceilings and walls, and that of cooling floors is about 80% which is a little higher than cooling ceilings and walls, which is caused by dropped cooled air deteriorating the convective heat exchange between radiant surfaces and indoor air.

For hybrid systems combined capillary mat cooling and displacement ventilation, it can be concluded that water supply temperature (T_{in}) and air supply volume have a great influence on the thermal environment through visual analysis and variance analysis with the confidence of 95% and 90%,% respectively, but the effect of air supply temperature is insignificant. The optical parameters settings are 23 °C air supply temperature, 18 °C air supply temperature and 2 times/h air supply volume taking account of energy consumption and desired indoor thermal environment.

The large time delay of the radiant cooling systems in the response phase is the main disadvantage comparing with conventional air-conditioning systems. The research on the response rate of the indoor air temperature can provide a reference for the proposal of a better control strategy. Furthermore, Significance analysis of parameters is the basis of regulation and management optimization for hybrid systems combining radiant and displacement ventilation.

Acknowledgments

This research is supported by the China National Key R&D Program “Energy-saving design and key technical equipment development for clean air-conditioning plants” (Grant number 2018YFC0705206), the Fundamental Research Funds for the Central Universities (Grant number 2018CDJDCH0015) and China Scholarship Council (Grant number 201806050245).

References

Awbi, H.B., 1998. Energy Efficient: Room Air Distribution. Elsevier Science Ltd, pp. 293–299.
Babayigit, O., Ozgoren, M., Aksoy, M.H., Kocaaslan, O., 2017. Experimental and CFD investigation of a multistage centrifugal pump including leakages and balance holes. Desalination Water Treat. 67, 28–40.
Causone, F., Corgnati, S.P., Filippi, M., Olesen, B.W., 2009. Experimental evaluation of heat transfer coefficients between radiant ceiling and room. Energy Build. 41 (6), 622–628.
ASHRAE, 2000. HVAC Systems and Equipment Handbook. Chapter 6: Panel Heating and Cooling, American Society of Heating Refrigeration and Air-conditioning Engineers. USA.
Cholewa, T., Rosinski, M., Spik, Z., Dudzinska, M.R., Siuta-Olcha, A., 2013. On the heat transfer coefficients between heated/cooled radiant floor and room. Energy Build. 66, 599–606.
Feng, J., Schiavon, S., Bauman, F., 2013. Cooling load differences between radiant and air systems. Energy Build. 65, 310–321.
Feustel HE, S.C., 1995. Hydronic radiant cooling-preliminary assessment. Energy Build. 22, 193–205.
Hu, R., Niu, J.L., 2012. A review of the application of radiant cooling & heating systems in mainland China. Energy Build. 52, 11–19.
Jinliang, W., 1999. Analysis of evaporation heat transfer mechanism in capillary tubes. J. Chem. Ind. Eng. (China) 50, 435–442.
Karmann, C., Schiavon, S., Bauman, F., 2017. Thermal comfort in buildings using radiant vs. all-air systems: a critical literature review. Build. Environ. 111, 123–131.
Kilkis, L.B., Sager, S.S., Uludag, M., 1994. A simplified model for radiant heating and cooling panels. Simul. Pract. Theory 2, 61–76.
Kim Wufeng, Y.M., Guangyu, J., 2010. Experimental study on cooling performance of capillary network system. Heat. Vent. Air Cond. 9, 102–106.
Koca, A., Gemici, Z., Topacoglu, Y., Cetin, G., Acet, R.C., Kanbur, B.B., 2014. Experimental investigation of heat transfer coefficients between hydronic radiant heated wall and room. Energy Build. 82, 211–221.
Koichi Kitagawa, N.K., 1999. Effect of humidity and small air movement on thermal comfort under a radiant cooling ceiling by subjective experiment. Energy Build. 30, 185–193.
Lim, J.-H., Jo, J.-H., Kim, Y.-Y., Yeo, M.-S., Kim, K.-W., 2006. Application of the control methods for radiant floor cooling system in residential buildings. Build. Environ. 41 (1), 60–73.
Mundt, E., 1995. Displacement ventilation systems–convection flows and temperature gradients. Build. Environ. 30, 129–133.
Ning, B., Schiavon, S., Bauman, F.S., 2017. A novel classification scheme for design and control of radiant system based on thermal response time. Energy Build. 137, 38–45.
Okamoto, S., Kitora, H., Yamaguchi, H., Oka, T., 2010. A simplified calculation method for estimating heat flux from ceiling radiant panels. Energy Build. 42 (1), 29–33.
Rees, S.J., Haves, P., 2013. An experimental study of air flow and temperature distribution in a room with displacement ventilation and a chilled ceiling. Build. Environ. 59, 358–368.
Ren Jie, L.H., Jingming, Z., 2008. Application and promotion of capillary network plane radiation air conditioning system. China Constr. Heat. Refrig. 6, 27–29.
Rhee, K.-N., Kim, K.W., 2015. A 50 year review of basic and applied research in radiant heating and cooling systems for the built environment. Build. Environ. 91, 166–190.
Richard, K., Strand, K.T.B., 2005. Modeling radiant heating and cooling systems: integration with a whole-building simulation program. Energy Build. 37, 389–397.
Richard, K., Strand, P.D., 2003. Investagation of a condenser-linked radiant cooling system using a heat balance based energy simulation program. ASHRAE 37, 389–397.
Roshan, G.R., Farrokhzad, M., Attia, S., 2017. Defining thermal comfort boundaries for heating and cooling demand estimation in Iran's urban settlements. Build. Environ. 121, 168–189.
Sarker, D., Jeong, J.H., 2012. Development of empirical correlations for non-adiabatic capillary tube based on mechanistic model. Int. J. Refrig. 35 (4), 974–983.
Shao, L.-L., Wang, J.-C., Jin, X.-C., Zhang, C.-L., 2013. Assessment of existing dimensionless correlations of refrigerant flow through adiabatic capillary tubes. Int. J. Refrig. 36 (1), 270–278.
Shuzo Murakami, S.K., 2001. Indoor climate design based on CFD coupled simulation of convection, radiation, and HVAC control for attaining a given PMV value. Build. Environ. 36, 701–709.
Skistad, H., 1996. Displacement Ventilation. Research Studied Press Ltd, UK.
Song, D., Kim, T., Song, S., Hwang, S., Leigh, S.-B., 2008. Performance evaluation of a radiant floor cooling system integrated with dehumidified ventilation. Appl. Therm. Eng. 28 (11–12), 1299–1311.
Stetiu, C., 1999. Energy and peak power savings potential of radiant cooling systems in US commercial buildings. Energy Build. 30, 127–138.
Taeyeon Kim, S.K., 2001. Indoor cooling/heating load analysis based on coupled simulation of convectionn, radiation and HVAC control. Build. Environ. 36, 901–908.
Watson, R.D., Chapman, K.S., 2002. Radiant Heating and Cooling Handbook. McGrawHill, New York.
Xiaxiong Yuan, Q.C., Glickman, L.R., 1998. A critical review of displacement ventilation. In: Proceedings of the ASHRAE Transactions.
Xing, H., 2001. A study of the air quality in the breathing zone in a room with displacement ventilation. Build. Environ. 36, 809–820.
Xing, H., 2002. Measurement and calculation of the neutral height in a room with displacement ventilation. Build. Environ. 37, 961–967.
Yang, L., Wang, W., 2008. A generalized correlation for the characteristics of adiabatic capillary tubes. Int. J. Refrig. 31 (2), 197–203.
Zhang, L., Liu, X.-H., Jiang, Y., 2013. Experimental evaluation of a suspended metal ceiling radiant panel with inclined fins. Energy Build. 62, 522–529.
Zhao, K., Liu, X.H, Jiang, Y., 2016. Application of radiant floor cooling in large space buildings – a review. Renew. Sustain. Energy Rev. 55, 1083–1096.